Title

Polytetrafluorethylene (PTFE) burn characteristics and toxicant formation in an oxidizer cross-flow via laser absorption tomography

Journal

Proceedings of the Combustion Institute, 40(1-4)

ISSN

1540-7489

Authors

Sanders, Isabelle C
Oberlander, Katherine A
Spearrin, R Mitchell

Publication Date

2024

DOI

10.1016/j.proci.2024.105394

Polytetrafluorethylene (PTFE) burn characteristics and toxicant formation in an oxidizer cross-flow via laser absorption tomography

Isabelle C. Sanders[a,*], Katherine A. Oberlander[a], R. Mitchell Spearrin[a]

[a] *Department of Mechanical and Aerospace Engineering, University of California, Los Angeles (UCLA), Los Angeles, California, 90095*

Abstract

A two-dimensional solid-fuel combustion experiment for fire-resistant polymers under forced convective cross-flow was developed to assess burn characteristics and toxicant formation using advanced laser absorption diagnostics that enable in situ species and temperature measurements near the fuel surface. The method was used to examine the thermochemical flow-field structure near the surface of polytetrafluoroethylene (PTFE) exposed to a well-defined solid-fuel pilot flame burning polymethyl methacrylate (PMMA). Infrared diode and quantum cascade lasers were used to probe rovibrational absorption transitions of hydrogen fluoride (HF) and carbon monoxide (CO), respectively, at the exit plane of a heterogeneous cylindrical fuel grain from which temperature and mole fraction could be inferred. A laser absorption tomography (LAT) technique with a Tikhonov-regularized Abel inversion was applied to reconstruct radially-resolved profiles in the axisymmetric reacting flow which, when compiled across a range of fuel lengths, provided a two-dimensional image of the near-surface reaction layer. Thermochemical data and reaction rate parameters from existing fluorocarbon chemistry models were used to generate high-temperature simulations of product species concentrations and temperature as a function of oxidizer-to-fuel ratio to elucidate observed trends and identify key reactions relevant to the novel dataset. The geometry and scale of the composite fuel experiments is intended to be tractable for reactive multi-physics models, enabling quantitative comparison of combustion characteristics and ultimately improved predictive capability of toxicant quantities resulting from fluoropolymer combustion in fire environments.

Keywords: fluorocarbon combustion; laser absorption spectroscopy; fire-resistant polymers; hydrogen fluoride

1. Introduction

Fire-resistant polymers are used extensively in modern structures to reduce flammability and the probability of fire-related loss or death. However, gas-phase emissions from these materials are often more toxic than those from conventional fuels. Specifically, halogenated polymers are considered fire resistant due to their chemical stability at high temperatures and the release of halides or halogen acids which can interfere with gas-phase combustion and limit heat release [1]. Unfortunately, hydrogen halides are acutely toxic and incomplete combustion leads to elevated emissions of carbon monoxide and unburned hydrocarbons including aromatics. These toxicants significantly increase the health and safety risk associated with smoke inhalation for first responders and civilians in close proximity to structural fires. While these challenges are well known, the detailed physics (kinetics, transport) associated with toxicant formation are insufficiently understood for many halogenated polymers, precluding accurate model prediction of fire toxicity and inhibiting risk quantification.

Polytetrafluoroethylene (PTFE), or Teflon, is a common fire-resistant fluoropolymer used extensively in construction and industrial applications due to its chemical inertness and high-temperature stability. The stability of PTFE may be attributed to the carbon-fluorine bond associated with the monomer tetrafluoroethylene (C_2F_4). The bond dissociation energy of the C–F single bond is higher than any other carbon-halogen as well as carbon-hydrogen bonds. As such, the pyrolysis of PTFE requires higher temperatures than most other synthetic or natural polymers and the material does not easily burn. However, upon thermal decomposition of PTFE in a fire environment, fluorine and fluorocarbon radicals will form and participate in combustion. Fluorine has the highest electronegativity of any element, and thus strongly attracts shared electrons, more so than oxygen. In the presence of H_2O, which is common to any ambient or fire environment, fluorinated radicals will react to form hydrogen fluoride (HF). HF is an acutely toxic gas with a lethal human exposure limit of approximately 50 ppm for a 30 minute period [2]. Here we aim to examine the incipient formation of HF (as well as CO) and associated burn characteristics of PTFE at fire conditions.

A number of previous theoretical and experimental studies have examined fluorocarbon combustion to advance chemical models towards predictive capability of toxicant formation. The foundational shock tube studies by Modica and LaGraff introduced a simple two-step mechanism to capture high-temperature C_2F_4 pyrolysis and oxidation, respectively, determining formation rates of CO and F atoms [3]:

$$C_2F_4 \longrightarrow 2CF_2 \quad \text{(R1)}$$

$$CF_2 + O_2 \longrightarrow CO + 2F + O \quad \text{(R2)}$$

Subsequent studies have built more detailed reaction mechanisms that account for additional steps and pathways for pyrolysis, oxidation, and hydrogen interactions, with the latter required to predict HF. Modeling hydrofluorocarbon chemistry has required more sophisticated theoretical approaches to determine the many potential reaction pathways. Burgess et al used a combination of empirical data and ab initio calculations to produce a comprehensive mechanism of C1 and C2 fluorinated hydrocarbon chemistry [4], which has been tested and modified in other works [5–7]. Recent efforts towards understanding high-temperature hydrofluorocarbon chemistry have included shock tube studies to interrogate additional pyrolysis pathways [8, 9] and refined calculations of thermochemical properties [10, 11]. To ultimately predict toxic emissions in a realistic fire environment, additional physics including heat transfer mechanisms and fluid dynamics must be considered, and coupled with the chemistry. State-of-the-art computational studies have recently shown promise to couple such detailed chemistry with multi-dimensional solid-fuel combustion models [12–14]. Complementary and computationally tractable experiments are needed with quantitative in situ measurements of species, temperature, and other spatially-evolving parameters to constrain and anchor such models.

In this work, we present a solid-fuel combustion experiment for fire-resistant polymers subject to forced convective cross-flow to assess burn characteristics and toxicant formation from PTFE using laser absorption diagnostics for in situ species and temperature measurements near the fuel surface. The paper first describes the axi-symmetric solid-fuel experimental configuration and optical diagnostic integration, which involves an oxygen-enriched pre-burner flame using polymethyl methacrylate (PMMA) to create well-defined high-temperature boundary conditions to which the PTFE is exposed. The laser absorption tomography methods are then detailed, highlighting the advantage of the axi-symmetric geometry to reconstruct quantitative two-dimensional images of thermochemical flow structure near the material surface. A novel dataset of quantitative hydrogen fluoride and carbon monoxide species profiles as well as temperature is presented. The results are discussed with an accompanying first-order analysis using available thermochemical models that describe high-temperature chemical reaction pathways for fluorocarbon oxidation in a fire-like environment.

2. Methods

2.1. Solid Fuel Burner

The solid-fuel combustion experiment was adapted from our prior work [15] and is shown in Fig. . The experiment involves forced convection of a gaseous oxidizer across a cylindrical solid fuel grain. The cylindrical grain geometry provides 2D axi-symmetry (r,z) of the gas-solid interface, enabling quantitative tomographic reconstruction of line-of-sight optical measurements from a single view angle (discussed further below) while avoiding the edge ef-

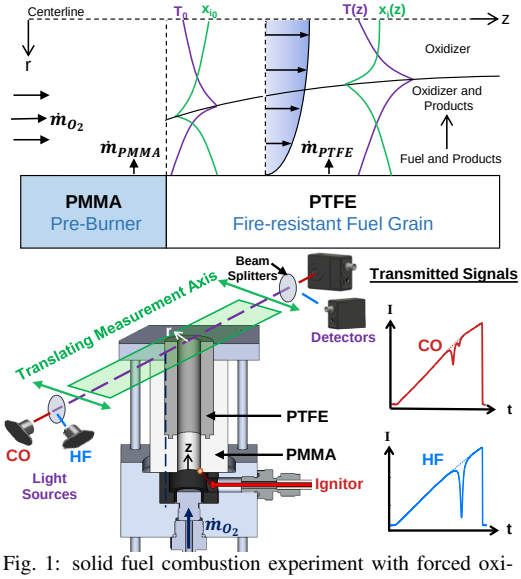

Fig. 1: solid fuel combustion experiment with forced oxidizer convection and laser absorption tomography setup enabling two-dimensional measurements.

fects of planar slab burners. The cylindrical axisymmetry also provides a relatively simple geometry for detailed computational modeling [12]. The test rig is designed to accommodate fuel grains of varying composition and length, the latter of which enables two-dimensional measurements based on exit plane measurements at different axial distances (z). Due to the high-temperature stability and fire resistance of PTFE, a composite fuel grain assembly was used in place of a homogeneous fuel cylinder. Notably, PTFE combustion proved difficult to initiate even in a pure oxygen environment at ambient temperature. As such, a 25.4 mm (1 in.) long polymethyl methacrylate (PMMA) fuel grain was used as a pilot burner to expose PTFE to both sustained high temperatures that initiate pyrolysis as well as hydrocarbon combustion product gases typically present in fires. PTFE fuel grains from 12.7-127mm (0.5-5 in.) in length were examined, each mated to the top surface of the PMMA pilot fuel grain. The boundary condition (temperature, species) created by the preburner was characterized, as shown in Fig. 5 and held constant across experiments. Importantly, the PMMA pre-burner combustion facilitates HF formation by supplying hydrogen (via water vapor) to the oxygen-enriched core flow with which the fluorocarbons can react, as would be the case in a fire environment. The test rig, and all associated experimental components, were contained within a high-flow (1150 cfm) laboratory fume hood to exhaust combustion products.

The composite fuel grain, including both the PTFE and PMMA components, had an inner diameter of 12.7 mm (0.5 in.). All tests were performed with a consistent oxidizer mass flow rate of $\dot{m}_{ox} = 1.5$ g/s using a single central injection port previously characterized [16]. Ignition was controlled remotely with an electrically-initiated pyrotechnic charge directed into a precombustion chamber directly beneath the bottom surface of PMMA [15]. The mass of the heterogeneous fuel grain was measured before and after each test to estimate a test time-integrated mass loss, equivalence ratio and regression rate. A graphite gasket ($\sim$3 mm thick) was moulded to the top of the PTFE component to mitigate top surface pyrolysis. Burn durations for tests, including start up time and the quasi steady-state measurement period, were approximately 14 seconds. At the end of the test time, nitrogen gas was immediately flushed through the oxygen line to extinguish the flame and purge the plumbing.

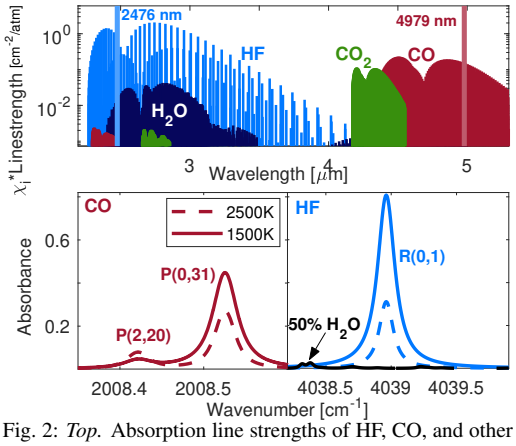

Fig. 2: *Top.* Absorption line strengths of HF, CO, and other relevant combustion species simulated at 2500 K [17]. *Bottom.* Simulated target transitions of CO and HF ($X = 15\%$) with exaggerated water interference.

2.2. Laser Absorption Spectroscopy

In situ species and temperature measurements in the near-surface reaction layer were performed using infrared laser absorption spectroscopy (LAS). LAS relates the attenuation of light through a gas medium to thermophysical properties of the absorbing molecules. Species-specific absorption spectra can be obtained by tuning lasers in spectral frequency or wavelength across individual lines associated with quantum energy transitions of the species of interest. In this study, we probe the mid-infrared fundamental vibrational bands of HF and CO in order to quantitatively recover species mole fraction and temperature in the reacting flow. The targeted wavelengths or frequencies are highlighted in Fig. 2. Specifically, we probe the hydrogen fluoride spectra in the R-branch of the fundamental band near 2475 nm. The R(1) rovibrational line at 4038.965 cm^{-1}, simulated in Fig. 2, was selected due to its high strength and lack of spectral interference from other atmospheric and combustion gases. It should be noted that non-optical ex situ detection and quantification of HF is particularly difficult due to its propensity to irreversibly interact with solid surfaces associated with sensors and sampling [18]. For carbon monoxide, we probe the P(0,31) and P(2,20) transitions near 2008.5 cm^{-1}

as also shown in Fig. 2. This line pair can be measured simultaneously within the typical injection current tuning range of a semi-conductor laser. The CO lines were selected in part due to the large difference in lower state energies, $\Delta E" = 3151\text{cm}^{-1}$, which enhances temperature sensitivity [15]. We note the spectroscopic parameters of all target transitions are compiled in the HITRAN database [17].

The laser spectroscopy optical setup was coupled with the solid fuel combustion test rig as depicted in Fig. . A distributed feedback (DFB) diode laser (Norcada) with ∼5 mW output centered around 4040 cm^{-1} was utilized to target the hydrogen fluoride line. For carbon monoxide, a DFB quantum cascade laser (Alpes) with ∼75 mW output centered around 2008 cm^{-1} was used. The output beams of both lasers were combined via a CaF_2 beam splitter to make them co-linear before being focused across the exit plane of the fuel grain with a beam waste of ∼0.5 mm. On the catch side, a second beam splitter was used to spatially de-multiplex the colinear beams, producing two perpendicular beams. Narrow bandpass spectral filters were placed along the separate beam paths to isolate each wavelength in front of distinct photodetectors (VIGO PVI-4TE-5 and Thorlabs PDA10D) used for CO and HF measurements. Both lasers were injection-current scanned in intensity and wavelength at a frequency of 2 kHz using a sawtooth waveform, while the transmission signals from the photodetectors were recorded at a 2.5 MHz sample rate. The multi-plexed optical line of sight was translated at 2.5 mm/s across the exhaust plane. The recorded transmission signals were time-averaged (every 200 scans) to yield a measurement radial resolution of half the beam diameter, such that the beam diameter (0.5 mm) effectively determines the radial spatial resolution.

2.3. Tomographic Imaging

Attaining the spatial profiles of temperature and species involves a tomographic inversion of the path-integrated line-of-sight laser absorption signals. Each of the three target lines for HF and CO are spectrally-resolved via the laser scans. The intensity signals can be converted to spectral absorbance, $\alpha(\nu)$, and spectrally integrated to yield projected absorbance areas, A_{proj}, for each target line, spatially-resolved across the measurement plane (see figure 3, top). These spatially-resolved path-integrated line areas, A_{proj}, can be directly related to the line-of-sight distribution of the integrated spectral absorption coefficient, $K(l)$:

$$A_{\text{proj}}(y) = \int_{-\infty}^{\infty} \alpha(\nu)\text{d}\nu = \int_{0}^{L(y)} K(l)\text{d}l = \int_{0}^{L(y)} PS_j(T(l))X_i(l)\text{d}l \quad (1)$$

To invert the line-of-sight absorption measurements, we exploit the axisymmetry of the flow-field to employ a Tikhonov-regularized onion peeling deconvolution [15, 16, 19], commonly referred to as 1D tomography, to convert the projected absorbance areas to line-integrated spectral absorption coefficients, $K(r)$, in the radial dimension (see figure 3, bottom). The Tikhonov regularization (or smoothing) parameter was tuned through assessment of the L-curve to balance over-fitting versus over-smoothing. The radially-resolved ratio of the integrated absorption coefficients of the two CO lines is used to obtain temperature, $T(r)$, where the ratio reduces to a linestrength ratio that is only a function of temperature: $R(r) = K_1(r)/K_2(r) = S_1(T(r))/S_2(T(r))$. With the gas temperature distribution known, the radially-resolved mole fraction can be determined from the radially-resolved spectral absorption coefficient of a single line via: $X(r) = K_j(r)/PS_jT(r)$. To produce two-dimensional images of the reaction layer, the radial absorption profiles were acquired at different axial lengths of the PTFE fuel grain, while holding the PMMA pre-burner length and oxidizer flow rate constant.

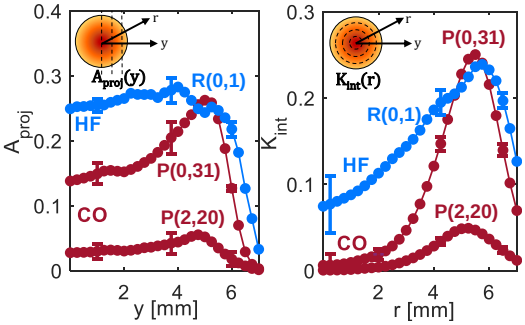

Fig. 3: *Left.* Projected integrated absorbance area verses distance y from the center of the reacting flow. *Right.* Tomographically-inverted radially-resolved integrated absorption coefficient.

3. Results

Experiments were conducted for PTFE fuel grain lengths of 25.4mm–127mm (1–5 in.) with 25.4 mm (1 in.) interval spacing, with an additional test of a 12.7 mm (0.5 inch) fuel grain to add spatial resolution in a region where a higher gradient was expected near the PMMA boundary condition. The forced convection oxidizer flow rate was held constant at $\dot{m}_{ox} =$ 1.5 g/s. Several tests were conducted at a single fuel grain length to verify experimental repeatability and to assess the quasi-steady state and axisymmetric assumptions over the measurement time.

Global fuel regression behavior was assessed based on post-burn mass loss and geometric measurements of the fuel grain; key results of this analysis are presented in Table. 1. The total consumed fuel mass was determined for each of the PMMA pilot burner and the PTFE fuel grain by measuring the masses before and after each hot-fire test. This mass loss is used along with the total burn time to determine the space-time averaged parameters discussed. The space-time averaged regression rate, $\bar{\dot{r}}$, is observed to decrease with fuel grain length due to the declining availability

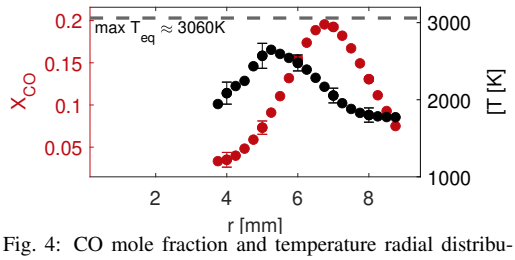

Fig. 4: CO mole fraction and temperature radial distribution measured from the 25.4 mm long PMMA pilot burner in GOx cross-flow.

of oxygen from ongoing reactions and formation of oxygenated product species. The averaged mass burn rate of regressing PTFE with fuel grain length are also shown. The rates were corrected for burn time variation by accounting for variation in mass burn rates measured from the 25.4 mm (1 in.) PMMA pilot burner fuel grain which ranged from 0.22 +/- 0.03 g/s. Over axial length, we observe a diminishing marginal increase in $\dot{m}$, consistent with the declining regression rate. Compared to a study with PMMA as the sole fuel, the rates measured for PTFE regression are over 50% lower [16]. The oxidizer-to-fuel (O/F) ratio decreases with fuel grain length as fuel mass is added to the constant oxidizer mass flow, trending from fuel-lean towards fuel-rich conditions. These global burn characteristics, although space-time averaged, provide an important reference for more granular species and temperature measurements.

Table 1: Global fuel regression parameters for PTFE with PMMA/GOx pre-burner and $\dot{m}_{ox} = 1.5$ g/s

L_f in.	$\bar{r}$ [mm/s]	$\bar{G}$ [kg/m^{2}s]	$\bar{\dot{m}}_{PTFE}$ [g/s]	O/F$\|_{t_b}$
0.5	0.069	0.010	0.17	9.8
1	0.041	0.011	0.23	7.6
2	0.039	0.012	0.35	5.1
3	0.024	0.014	0.44	3.0
4	0.021	0.014	0.55	3.1
5	0.017	0.015	0.58	2.2

3.1. PMMA pre-burner boundary condition

The pre-burner boundary condition was measured using the laser absorption measurements with the 1D tomography deconvolution method to determine the initial temperature and gas composition to which the PTFE was exposed. The first subplot in Fig. 5 shows the measured temperature and CO species as a function of radial position from the core. Given the PMMA mass burn rate, the global equivalence ratio at the boundary was approximately $\phi = 0.28$. Despite this very fuel-lean global condition, a peak temperature (∼2950 K) slightly lower than the stoichiometric value is reached within 4 mm of the fuel surface due to the radial distribution of O/F ratio moving from fuel rich at the surface to the core which is primary oxygen. The carbon monoxide mole fraction is measured

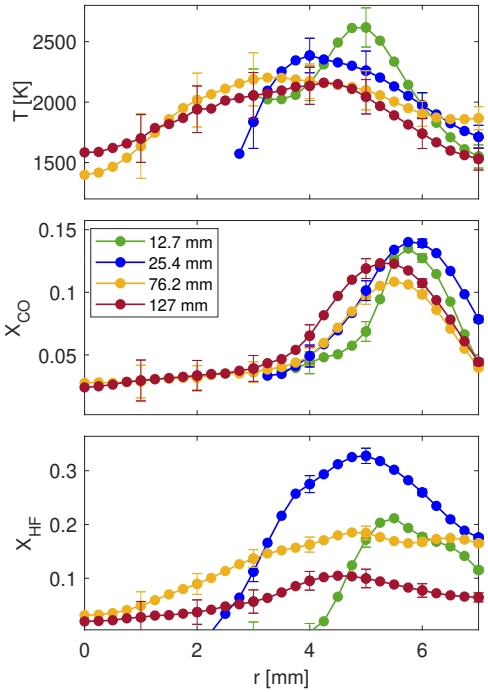

Fig. 5: Planar species and temperature measurements for PTFE combustion along the radial dimension at different axial measurement planes.

to peak at nearly 20% within 2 mm of the fuel surface while reducing to nearly zero within 5 mm of the PMMA surface. Overall, based on the global O/F, it is estimated that approximately 50-60% of the bulk cross-flow remains oxygen.

3.2. PTFE reaction layer measurements

Laser absorption tomography results from the aforementioned combustion tests of PTFE with the hot vitiated oxygen cross-flow are shown for select axial distances in Fig. 5 and compiled across the full experimental domain in two-dimensional images in Fig. 6. Quantitative spatially-resolved temperature and species profiles illustrate the thermochemical evolution in the reaction layer. Select trends are noted here and discussed further in the following section. It is notable that due to the inherently faster fuel regression of PMMA compared to PTFE, the respective port diameters and thus radial domains differ, rendering a slight flow convergence at the interface. Temperature and species uncertainty, as represented by error bar magnitudes, reflects variation in axisymmetry across the flow centerline, uncertainty associated to tomographic deconvolution, and uncertainty in spectral parameters from HITRAN [17]. Further details on this uncertainty analysis can be found in previous works from our group [16, 19].

Radial temperature distributions indicate a decrease in peak temperature and broadening with axial distance reflecting radial diffusion and mixing. The radial location of the peak temperature shifts towards

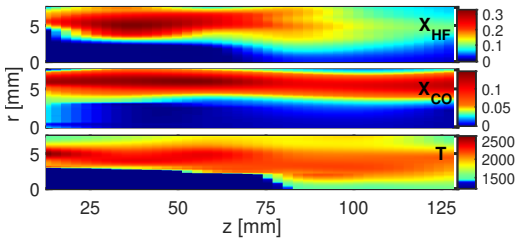

Fig. 6: Two-dimensional thermochemical structure in the near-surface reaction layer of PTFE in an oxidizer cross-flow

the oxygen-enriched core flow with increased axial distance as the O/F ratio decreases. The first measurement downstream of the fuel interface, at 12.7 mm (0.5 in.), most closely resembles the temperature profile measured at the PMMA surface initial condition. For the first few axial distances, there is insufficient concentration of carbon monoxide in the core flow (near $r = 0$) to obtain a reliable temperature measurement, thus the profiles are not fully-resolved. Moving downstream, more CO has been produced and has diffused into the core region such that local temperature can be calculated, albeit with greater uncertainty than in the more fuel and product rich regions near the fuel surface. The axial temperature decrease can also be attributed to increased distance from the PMMA pilot burner, and lower expected heat release of PTFE relative to PMMA.

The species measurements reflect an abundance of toxicant formation in the reaction layer, with HF reaching localized mole fraction values above 30%, and CO mole fraction peaking near 15%. In the bottom-right plot of Fig. 5, we observe an trend in X_{HF} with two distinct temporal phases. From the first to second measurement locations beyond the PMMA-PTFE interface where the gas is hottest, spanning 12.7 - 25.4 mm, the peak concentration of HF increases significantly and shifts about 0.5 mm towards the core. Beyond this point, however, we observe a decrease in peak HF concentration coupled with a rapid broadening across the radial domain. The more concentrated peaks seen at shorter lengths appear to spread out from their maxima a few millimeters inward of the fuel grain wall and distribute into the oxidizer core flow, though the concentrations in the core remain relatively low (X<0.05) throughout the range of fuel lengths tested. Conversely, the high CO concentrations are largely maintained with increasing axial distances, likely reflecting a balance of radial diffusion with increasing CO formation with lower O/F. Throughout the full axial domain, encompassing 127 mm, the peak CO location moves gradually towards the core for a total variation of approximately 1 mm.

4. Discussion/Analysis

The measured species and temperature results discussed in the prior section reflect radial and axial variation of O/F as well as chemical reaction kinetics that compete with the transport timescales. To assess the observed trends, a thermochemical equilibrium model and chemical kinetics mechanism were used to simulate relevant conditions. Simulations were performed using 0-D reactors in the Cantera toolbox, with hydrofluorocarbon thermodynamic data and reaction rate parameters from Burgess et al. [6, 7].

4.1. Chemical equilibrium analysis

To estimate chemical equilibrium for PTFE combustion with the pilot PMMA burner, a two-step simulation was performed. First a chemical equilibrium simulation of PMMA and oxygen was used to obtain product gas composition over a range of O/F reflecting the radial variation of O/F at the PMMA-PTFE boundary. Second, PMMA-O_2 product gas was used to prescribe the vitiated oxidizer initial conditions for PTFE combustion, using the TFE monomer as the primary fuel. The final simulated product composition is presented here in Figure 7 as a function of the experimental range of mass burn rates of PTFE, reflecting an increase in axial distance and corresponding reduction in O/F, which is similarly expected in radial variation moving towards the PTFE surface. The subplots show resulting composition for different initial equivalence ratios of MMA/GOx, representative of the radially-varied initial conditions [20]. The final subplot of figure 7 indicates the maximum temperature (for any O/F) expected at equilibrium based on the ratio of PTFE and PMMA mass consumption rates at different axial distances, where as $\dot{m}_{PTFE} \rightarrow 0$, the temperature would be the maximum temperature for pure PMMA. The simulations presented here are intended to provide a reference for the range of species concentration and temperatures measured in the PTFE reaction layer.

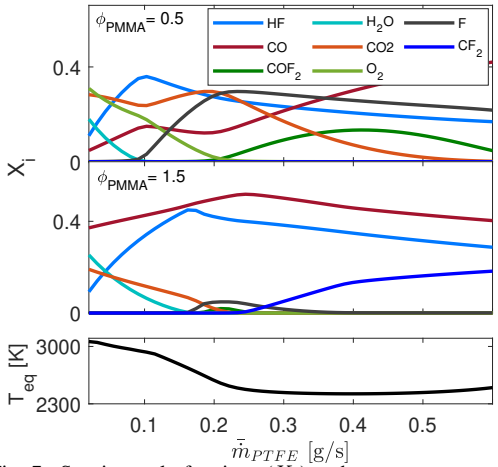

Fig. 7: Species mole fractions (X_i) and max temperature at chemical equilibrium, T_{eq}, for PTFE combustion over a range of mass flow rates of PTFE, with oxidizer vitiated with MMA/GOx products at equivalence ratios of 0.5 and 1.5.

Despite the relatively simplicity of the 0-D chemical equilibrium model, many of the observed trends in measured temperature and species are consistent. The maximum magnitude of HF mole fraction is simulated to be approximately 40% across the various

initial conditions, just higher than the maximum measured values. Notably, an initial spike in HF, peaking at fuel mass flow rates between 0.1 and 0.2 g/s, is followed by a gradual decay. This trend is reflected in the experimental data wherein the peak HF concentration increases between 12.7 mm and 25.4 mm, followed by a steady decline over the sequential axial positions. The initial rise is HF corresponds with a decline in H_2O, which is presumed the dominant hydrogen-containing species in the vitiated oxidizer exiting the PMMA-O_2 pilot burner. After HF peaks, the subsequent decline corresponds to a rise in atomic fluorine and carbonyl fluoride, COF_2, provided sufficient oxygen is present. The atomic fluorine and COF_2 concentrations decline at more fuel rich conditions, which become dominated by CO and CF_2, along with diluted HF, pronounced in the most oxygen-deficient initial condition. CO is predicted to form in large concentrations at most conditions. In comparison to the experimental measurements, the equilibrium model estimates notably higher peak CO concentrations ($\sim$40%) in the fuel-rich regions by about a factor of 2. Some of the difference can certainly be related to over-simplification of the model, but carbon predicted to form carbon monoxide and other gaseous products may also disproportionately exist in solid carbon char or particles.

The equilibrium temperature shown is the maximum value across the range of radial fuel-lean to fuel-rich equivalence ratios for a given global balance of PTFE and PMMA mass burn rates at each axial position. As $\bar{\dot{m}}_{PTFE} \rightarrow 0$, the maximum equilibrium temperature approaches that of purely MMA/GOx combustion, approximately 3060K. Downstream, further away from the PMMA fuel grain, the temperature decreases to a plateau of around 2350K which is slightly higher, but within uncertainty, compared to the experimentally measured temperatures downstream. Beyond the first 25.4 mm downstream, corresponding in the model to $\bar{\dot{m}}$ of approximately 0.2, the peak temperature stabilizes. These trends are consistent with experimental data. The formation of HF is exothermic, however, the formation, by way of fluorocarbon decomposition, of the F radical is endothermic. The effects of the trade off in these fluorinated end product species is seen in the temperature trend. As less hydrogen is available for F to abstract to form HF, F radical product concentration increases and the equilibrium temperature decreases. The formation of COF_2 is similarly endothermic, thus its concentration peaks also contribute to local lower temperatures in fuel lean conditions where it is most present.

4.2. Reaction kinetics analysis

To better understand the reactions responsible for the observed trends in species and temperature for PTFE combustion, a high-temperature chemical kinetic reaction pathway analysis was performed. Key pathways from PTFE to CO and HF formation at 2500 K are shown in figure 8. PTFE thermally decomposes at high temperatures ($> 400^{\circ}$C) primarily

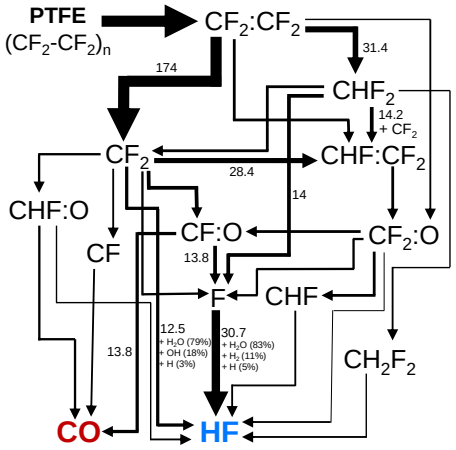

Fig. 8: Reaction pathway diagram tracking the fluorine atom through PTFE pyrolysis and oxidation with water along pathways that result in hydrogen fluoride (and carbon monoxide) production (T = 2500K)

into the monomer, tetrafluoroeythylene (TFE), from which numerous reaction pathways exist to form HF and CO as products by way of intermediate fluorocarbons, hydrofluorocarbons (HFCs), and carbon oxofluorides (COFs). As mentioned, the PMMA combustion products serve as the primary source of hydrogen, largely via water molecules, which is required in the formation of HF. The case shown reflects the relative reaction contributions simulated at an early time step of 2.5 μs for equal mass contributions from PTFE and PMMA (the pilot burner fuel) analogous to approximately 25.4 mm downstream of the PMMA/PTFE interface. Here, the PMMA contribution is again represented by the product species resulting from a prior equilibrium simulation of MMA/GOx where $\phi = 1$. While the relative contributions towards the formation of HF and CO are dependent on the initial fuel-oxidizer mixture and temperature, the case in Figure 8 was selected as it is representative of the many major contributing pathways found across initial conditions and reactor progression at combustion temperatures.

Beyond the initial depolymerization, TFE primarily decomposes into two difluoromethylene (CF_2) molecules, although some reacts to form difluoromethylide (CHF_2) and carbonyl fluoride (COF_2). The magnitude of these alternate pathways is directly impacted by the initial concentrations of H_2O and O_2 available as dictated by the preliminary MMA combustion equilibrium. The predominant pathways we observe here towards CO formation involve the oxidation of CF_2 to produce the carbon oxofluorides, CFO and CH:FO, followed by decomposition (see R3 and R4 below); the reaction following the latter species also produces HF.

$$\text{CF:O} \longrightarrow \text{CO} + \text{F} \qquad \text{(R3)}$$

$$\text{CHF:O} \longrightarrow \text{CO} + \text{HF} \qquad \text{(R4)}$$

Although the reaction rates (shown in $kmol/m^3s$) resulting in CO are shown to be relatively low compared to the pathways producing HF, this is largely due to the time step as the formation of HF is relatively rapid compared to that of CO.

The fluorocarbons, HFCs, and COFs nearly all have direct reactions that produce HF; however, the favored pathways consistently involve dissociation to produce the fluorine atom from these molecules. Thereafter, the highly reactive fluorine radicals rapidly abstract hydrogen from water and react with the hydrogen molecules and radicals to produce HF, per R5.

$$F + H_2O \longrightarrow OH + HF \qquad (R5)$$

Previous works have found, by way of modeling and experimental efforts, hydrogen fluoride to be formed preferably over water as a final endpoint product for hydrogen [5]. This is due to the relatively high electronegativity of fluorine and H-F bond strength, making it a more stable product of the two. In fact, provided there are sufficient fluorine atoms available, the chemical model predicts that any water present will decompose and the hydrogen atoms will react to form, as follows from the experimental HF trend and was noted in the equilibrium simulation results above.

5. Conclusion

In this work, the burn characteristics and toxicant formation of polytetrafluoroethylene (PTFE) combustion were examined using laser absorption tomography. Experiments were conducted in a solid fuel combustion facility with gaseous oxygen cross-flow and a PMMA pilot burner to emulate fire-like conditions. Radially-resolved temperature and species (CO and HF) concentration profiles were obtained by inverting line-of-sight absorption measurements across the fuel grain exit planes. Quantitative, two dimensional thermochemical images were produced by compiling planar results from tests with varied fuel grain lengths. The data were compared to chemical models for fluorocarbon thermal decomposition and combustion, revealing similar trends to the experimental results and highlighting the underlying reaction pathways responsible for some observations. The geometries, operating conditions, and experimental measurements of these experiments are detailed so that the data can serve as validation targets for higher-fidelity models of toxicant formation and destruction in PTFE combustion.

Declaration of competing interest

The authors declare that they have no known competing financial interests or personal relationships that could influence the work reported in this paper.

Acknowledgments

This work was funded by the U.S. Federal Emergency Management Agency (EMW-2021-FP-00199). ICS acknowledges support from the Natural Sciences and Engineering Research Council of Canada.

References

[1] P. Kiliaris, C. D. Papaspyrides, Polymers on Fire, in: C. D. Papaspyrides, P. Kiliaris (Eds.), Polymer Green Flame Retardants, Elsevier, Amsterdam, 2014, pp. 1–43.

[2] National Research Council, Hydrogen fluoride, in: Acute Exposure Guideline Levels for Selected Airborne Chemicals, Vol. 4, National Academies Press (US), 2004.

[3] A. P. Modica, J. E. LaGraff, Decomposition and Oxidation of C2F4 Behind Shock Waves, The Journal of Chemical Physics 43 (9) (2004) 3383–3392.

[4] D. R. Burgess, M. R. Zachariah, W. Tsang, P. R. Westmoreland, Thermochemical and chemical kinetic data for fluorinated hydrocarbons, Progress in Energy and Combustion Science 21 (6) (1995) 453–529.

[5] G. T. Linteris, G. W. Gmurczyk, Prediction of HF Formation During Suppression, Special Publication (NIST SP) - 890 2 (1995).

[6] D. R. Burgess Jr., V. I. Babushok, G. T. Linteris, J. A. Manion, A Chemical Kinetic Mechanism for 2-Bromo-3,3,3-trifluoropropene (2-BTP) Flame Inhibition, International Journal of Chemical Kinetics 47 (9) (2015) 533–563.

[7] D. R. Burgess Jr., V. I. Babushok, J. A. Manion, A chemical kinetic mechanism for combustion and flame propagation of CH2F2/O2/N2 mixtures, International Journal of Chemical Kinetics 54 (3) (2022) 154–187.

[8] C. J. Cobos, A. E. Croce, K. Luther, J. Troe, Shock Wave Study of the Thermal Decomposition of CF3 and CF2 Radicals, The Journal of Physical Chemistry A 114 (14) (2010) 4755–4761.

[9] C. J. Cobos, K. Hintzer, L. Sölter, E. Tellbach, A. Thaler, J. Troe, High-Temperature Fluorocarbon Chemistry Revisited, The Journal of Physical Chemistry A 125 (25) (2021) 5626–5632.

[10] D. S. J. Farina, S. K. Sirumalla, E. J. Mazeau, R. H. West, Extensive High-Accuracy Thermochemistry and Group Additivity Values for Halocarbon Combustion Modeling, Industrial & Engineering Chemistry Research 60 (43) (2021) 15492–15501.

[11] S. Sharma, K. Abeywardane, C. F. Goldsmith, Theory-Based Mechanism for Fluoromethane Combustion I: Thermochemistry and Abstraction Reactions, The Journal of Physical Chemistry A 127 (6) (2023) 1499–1511.

[12] C. Dhandapani, G. Blanquart, A. C. Karp, E. T. Jens, J. Rabinovitch, Combustion studies of MMA/GOx for a hybrid rocket motor, Combustion and Flame 256 (2023) 112994.

[13] A. Kacem, M. Mense, Y. Pizzo, G. Boyer, S. Suard, P. Boulet, G. Parent, B. Porterie, A fully coupled fluid/solid model for open air combustion of horizontally-oriented PMMA samples, Combustion and Flame 170 (2016) 135–147.

[14] A. Rampazzo, F. Barato, Modeling and CFD Simulation of Regression Rate in Hybrid Rocket Motors, Fire 6 (3) (2023) 100.

[15] F. A. Bendana, I. C. Sanders, J. J. Castillo, C. G. Hagström, D. I. Pineda, R. M. Spearrin, In-situ thermochemical analysis of hybrid rocket fuel oxidation via laser absorption tomography of CO, CO_2, and H_2O, Experiments in Fluids 61 (9) (2020) 190.

[16] I. C. Sanders, F. A. Bendana, C. G. Hagström, R. Mitchell Spearrin, Injector Effects on Hybrid Polymethylmethacrylate Combustion Assessed by Thermochemical Tomography, Journal of Propulsion and Power 37 (6) (2021) 928–943.

[17] I. Gordon, L. Rothman, R. Hargreaves, R. Hashemi, et al., The HITRAN2020 molecular spectroscopic database, Journal of Quantitative Spectroscopy and Radiative Transfer 277 (2022) 107949.

[18] R. Krebs, J. Owens, H. Luckarift, Formation and detection of hydrogen fluoride gas during fire fighting scenarios, Fire Safety Journal 127 (2022) 103489.

[19] C. Wei, D. I. Pineda, L. Paxton, F. N. Egolfopoulos, R. M. Spearrin, Mid-infrared laser absorption tomography for quantitative 2D thermochemistry measurements in premixed jet flames, Applied Physics B 124 (6) (2018) 123.

[20] F. A. Bendana, I. C. Sanders, N. G. Stacy, R. M. Spearrin, Localized characteristic velocity (c_*) for rocket combustion analysis based on gas temperature and composition via laser absorption spectroscopy, Measurement Science and Technology 32 (12) (2021) 125203.